4

Investigation of Mixing in Shear Thinning Fluids Using Computational Fluid Dynamics

Farhad Ein-Mozaffari and Simant R. Upreti
Ryerson University, Toronto
Canada

1. Introduction

Mixing is an important unit operation employed in several industries such as chemical, biochemical, pharmaceutical, cosmetic, polymer, mineral, petrochemical, food, wastewater treatment, and pulp and paper (Zlokarnik, 2001). Crucial for industrial scale-up, understanding mixing is still difficult for non-Newtonian fluids (Zlokarnik, 2006), especially for the ubiquitous shear-thinning fluids possessing yield stress.

Yield-stress fluids start to flow when the imposed shear stress exceeds a particular threshold yield stress. This threshold is due to the structured networks, which form at low shear rates but break down at high shear rates (Macosko, 1994). Many slurries of fine particles, certain polymer and biopolymer solutions, wastewater sludge, pulp suspension, and food substances like margarine and ketchup exhibit yield stress (Elson, 1988). Mixing of such fluids result in the formation of a well mixed region called cavern around the impeller, and essentially stagnant or slow moving fluids elsewhere in the vessel. Thus, the prediction of the cavern size becomes very important in evaluating the extent and quality of mixing. When the cavern size is small, stagnant zones prevail causing poor heat and mass transfer, high temperature gradients, and oxygen deficiency for example in aeration processes (Solomon et al., 1981).

The conventional evaluation of mixing is done through experiments with different impellers, vessel geometries, and fluid rheology. This approach is usually expensive, time consuming, and difficult. Moreover, the resulting empirical correlations are suitable only for the specific systems thus investigated. In this regard, Computational Fluid Dynamics (CFD) offers a better alternative. Using CFD, one can examine various parameters of the mixing process in shorter times and with less expense; an otherwise uphill task with the conventional experimental approach.

During the last two decades, CFD has become an important tool for understanding the flow phenomena (Armenante et al., 1997), developing of new processes, and optimizing the existing processes (Sahu et al., 1998). The capability of CFD to satisfactorily forecast mixing behavior in terms of mixing time, power consumption, flow pattern, and velocity profiles has been considered as a successful achievement. A distinct advantage of CFD is that, once a validated solution is obtained, it can provide valuable information that would not be easy to obtain experimentally. The objective of this work is to present recent developments in using CFD to investigate the mixing of shear-thinning fluids possessing yield stress.

2. CFD modeling of the mixing vessel

The laminar flow of a fluid in an isothermal mixing tank with a rotating impeller is described by the following continuity and momentum equations (Patankar, 1980; Ranade, 2002):

$$\frac{\partial \rho}{\partial t} = -\nabla . \rho v \tag{1}$$

$$\frac{\partial (\rho v)}{\partial t} = -\nabla \cdot (\rho v v) - \nabla p + \nabla \cdot \boldsymbol{\tau} + \rho g + F \tag{2}$$

where ρ, p, v, g, F and $\boldsymbol{\tau}$ respectively are the fluid density, pressure, velocity, gravity, external force, and the stress tensor given by

$$\boldsymbol{\tau} = \mu \left[(\nabla v) + (\nabla v)^T - \frac{2}{3} (\nabla \cdot v) I \right] \tag{3}$$

In the above equation, μ is the molecular viscosity, and I is the unit tensor. For incompressible fluids, the stress tensor is given by

$$\boldsymbol{\tau} = \mu \left[(\nabla v) + (\nabla v)^T \right] = \mu D \tag{4}$$

where D is the rate-of-strain tensor. For multidimensional flow of non-Newtonian fluids, the apparent viscosity (μ) is a function of all three invariants of the rate of deformation tensor. However, the first invariant is zero for incompressible fluids, and the third invariant is negligible for shearing flows (Bird et al., 2002). Thus, for the incompressible non-Newtonian fluids, μ is a function of shear rate, which is given by

$$\dot{\gamma} = \sqrt{\frac{1}{2} (D : D)} \tag{5}$$

It can be seen that $\dot{\gamma}$ is related to the second invariant of D.

2.1 The rheological model
Equations (1)–(5) need a rheological model to calculate the apparent viscosity of the non-Newtonian fluid. For shear-thinning fluids with yield stress, the following Herschel-Bulkley model has been widely used by the researchers (Macosko, 1994):

$$\mu = \frac{\tau_y}{\dot{\gamma}} + k |\dot{\gamma}|^{n-1} \tag{6}$$

where τ_y is the yield stress, k is the consistency index, and n is the flow behavior index. Table 1 lists the rheological parameters of aqueous xanthan gum solution, which is a widely used Herschel-Bulkley fluid (Whitcomb & Macosko, 1978; Galindo et al., 1989; Xuewu et al., 1996; Renaud et al., 2005).
The Herschel-Bulkley model causes numerical instability when the non-Newtonian viscosity blows up at small shear rates (Ford et al., 2006; Pakzad et al., 2008a; Saeed et al., 2008). This problem is surmounted by the modified Herschel-Bulkley model given by

$$\mu = \begin{cases} \mu_0 & \text{for} \quad \tau \le \tau_y \\ \dfrac{1}{\dot{\gamma}}\left[\tau_y + k\left(\dot{\gamma}^n - \left(\dfrac{\tau_y}{\mu_0} \right)^n \right) \right] & \text{for} \quad \tau > \tau_y \end{cases} \tag{7}$$

where μ_0 is the yielding viscosity. The model considers the fluid to be very viscous with viscosity μ_0 for the shear stress $\tau \le \tau_y$, and describes the fluid behavior by a power law model for $\tau > \tau_y$ (Ford et al., 2006; Pakzad et al., 2008a; Saeed et al., 2008).

xanthan gum concentration (%)	k (Pa.s^n)	n	τ_y (Pa)
0.5	3	0.11	1.79
1.0	8	0.12	5.25
1.5	14	0.14	7.46

Table 1. Rheological properties of xanthan gum solutions (Saeed & Ein-Mozaffari, 2008)

2.2 Simulation of impeller rotation

The following four methods exist for the simulation of impeller rotation in a mixing vessel:

The black box method requires the experimentally-determined boundary conditions on the impeller swept surface (Ranade, 1995). Hence, this method is limited by the availability of experimental data. Moreover, the availability of experimental data does not warrant the same flow field for all alternative mixing systems (Rutherford et al., 1996). The flow between the impeller blades cannot be simulated using this method.

The Multiple Reference Frame (MRF) method is an approach allowing for the modeling of baffled tanks with complex rotating, or stationary internals (Luo et al., 1994). A rotating frame (i.e. co-ordinate system) is used for the region containing the rotating components while a stationary frame is used for stationary regions. In the rotating frame containing the impeller, the impeller is at rest. In the stationary frame containing the tank walls and baffles, the walls and baffles are also at rest. The momentum equations inside the rotating frame is solved in the frame of the enclosed impeller while those outside are solved in the stationary frame. A steady transfer of information is made at the MRF interface as the solution progresses.

Consider the rotating frame at position r_0 relative to the stationary frame as shown in Figure 1. The rotating frame has the angular velocity $\boldsymbol{\omega}$. The position vector r from the origin of the rotating frame locates any arbitrary point in the fluid domain. The fluid velocities can then be transformed from the stationary frame to the rotating frame using

$$v_r = v - u_r \tag{8}$$

where v_r is the relative velocity viewed from the rotating frame, v is the absolute velocity viewed from the stationary frame, and u_r is the "whirl" velocity due to the moving frame given by

$$u_r = \boldsymbol{\omega} \times r \tag{9}$$

When the equation of motion is transferred to the rotating reference frame, the continuity and momentum equations respectively become
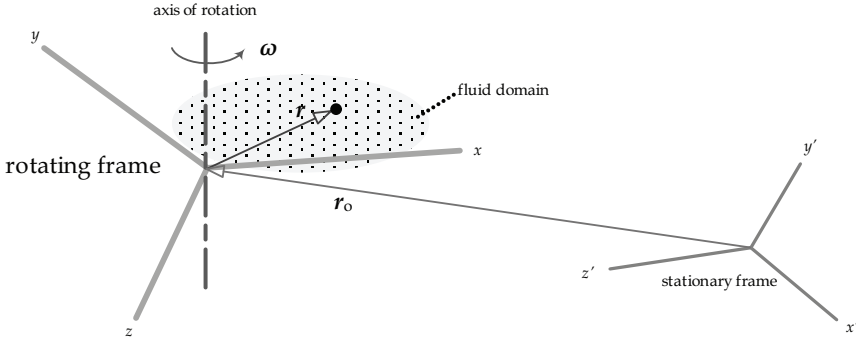
Fig. 1. The rotating and stationary frames

$$\frac{\partial \rho}{\partial t} = -\nabla.\rho v_{\mathrm{r}} \tag{10}$$

and

$$\frac{\partial(\rho v_{\mathrm{r}})}{\partial t} = -\nabla.\left(\rho v_{\mathrm{r}} v_{\mathrm{r}}\right) - \rho\left(2\boldsymbol{\omega}\times v_{\mathrm{r}} + \boldsymbol{\omega}\times\boldsymbol{\omega}\times r\right) - \nabla p + \nabla.\boldsymbol{\tau}_{\mathrm{r}} + \rho\boldsymbol{g} + \boldsymbol{F} \tag{11}$$

where $\left(2\boldsymbol{\omega}\times v_{\mathrm{r}}\right)$ and $\left(\boldsymbol{\omega}\times\boldsymbol{\omega}\times r\right)$ respectively are the Coriolis and centripetal accelerations, and $\boldsymbol{\tau}_{\mathrm{r}}$ is the stress tensor based on v_{r}. The momentum equation for the absolute velocity is

$$\frac{\partial(\rho v)}{\partial t} = -\nabla.\left(\rho v_r v\right) - \rho\left(\boldsymbol{\omega}\times v\right) - \nabla p + \nabla.\boldsymbol{\tau} + \rho\boldsymbol{g} + \boldsymbol{F} \tag{12}$$

where $\left(\boldsymbol{\omega}\times v\right)$ embodies the Coriolis and centripetal accelerations. The MRF method is recommended for simulations in which impeller-baffle interaction is weak. With this method, the rotating frame section extends radially from the centerline or shaft out to a position that is about midway between the blade's tip and baffles. Axially, that section extends above and below the impeller. In the circumferential direction, the section extends around the entire vessel.

The sliding mesh method is the most rigorous and informative solution method for stirred tank simulations. It provides a time-dependent description of the periodic interaction between impellers and baffles (Luo et al., 1993). The grid surrounding the rotating components physically moves during the simulations, while the stationary grid remains static. The velocity of the impeller and shaft relative to the moving mesh region is zero as is the velocity of the tank, baffles, and other internals in the stationary mesh region. The motion of the impeller is realistically modeled because the surrounding grid moves as well, enabling accurate simulation of the impeller-baffle interaction. The motion of the grid is not continuous, but it is in small discrete steps. After each such motion, the set of transport equations is solved in an iterative process until convergence is reached.

The snapshot method is based on snapshots of flow in a stirred tank in which the relative position of the impeller and baffles is fixed (Ranade & Dommeti, 1996; Ranade, 2002). The impeller blades are considered as solid walls, and the flow is simulated using stationary

frame in a fixed blade position. Simulations are performed at different blade positions, and the results averaged. Like the MRF method, the entire domain is divided into two regions. In the impeller region, time-dependent terms are approximated in terms of spatial derivatives. In the outer region, the relatively small time derivative terms can be neglected. Upon comparing numerical predictions obtained from applying different impeller modeling methodologies, several investigators observed that steady state methods such as MRF can

i.   provide reasonable predictions to flow field features and power consumption (Jaworski et al., 2001; Bujalski et al., 2002; Kelly & Gigas, 2003; Khopkar et al., 2004; Aubin et al., 2004; Sommerfeld & Decker, 2004; Khopkar et al., 2006), and

ii. save about one-seventh of the CPU-time (Brucato et al., 1998).

3. CFD model validation

For the mixing of shear-thinning fluids with yield stress, CFD model validation is typically done by comparing the CFD-predicted power number, and velocity field with the experimental counterparts (Ihejirica & Ein-Mozaffari, 2007; Saeed et al., 2007; Pakzad et al., 2008b; Ein-Mozaffari & Upreti, 2009).

Figure 2 depicts the impeller power number as a function of Reynolds number (Re) for the Lightnin A200 impeller in the mixing of xanthan gum solution, which is a shear-thinning fluid with yield stress (Saeed et al., 2008).
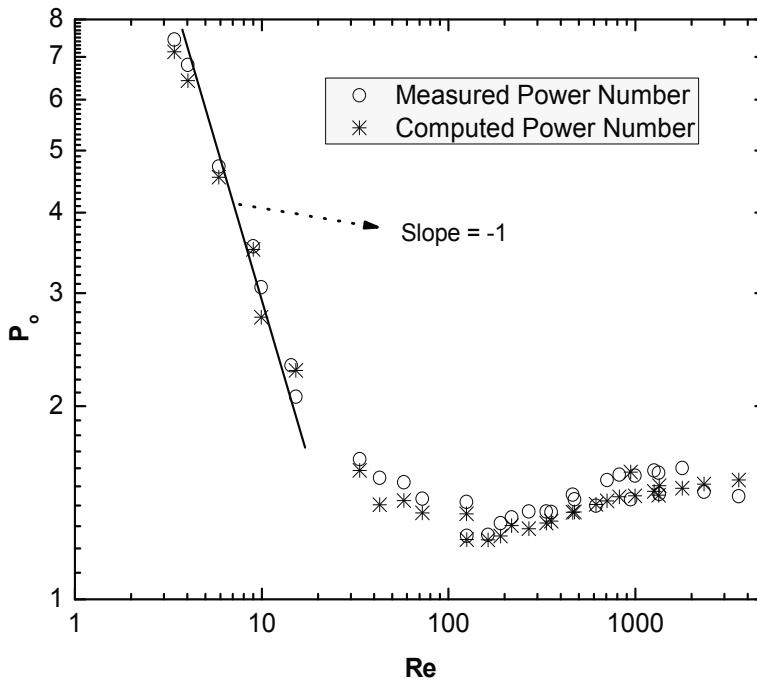

Fig. 2. Power number as a function of Reynolds number for the Lightnin A200 impeller

The power number is given by the following equation:

$$P_0 = \frac{P}{\rho N^3 D^5} \tag{13}$$

where P, N, D, and ρ respectively are power, impeller speed, impeller diameter, and fluid density. The Reynolds number is given by

$$\mathrm{Re} = \frac{\rho N^2 D^2 k_s}{\tau_y + k(k_s N)^n} \tag{14}$$

where τ_y is related to the average shear rate $\dot{\gamma}$ via the Herschel-Bulkley model as

$$\eta = \frac{\tau}{\dot{\gamma}} = \frac{\tau}{k_s N} = \frac{\tau_y + k(k_s N)^n}{k_s N} \tag{15}$$

and the average $\dot{\gamma}$ is given as follows (Metzner & Otto, 1957):

$$\dot{\gamma} = k_s N \tag{16}$$

The results illustrated in Figure 2 show a very good agreement between calculated power number and the experimentally determined values. At Re < 10 (the laminar regime), power number is inversely proportional to Re.

Comparison of velocity field To experimentally determine the velocity field, Ultrasonic Doppler Velocimetry (UDV) has been effectively used in the mixing of shear-thinning fluids with yield stress using different impellers (Ein-Mozaffari et al., 2007a, Ihejirika & Ein-Mozaffari, 2007; Saeed et al., 2008; Pakzad et al., 2008b; Ein-Mozaffari & Upreti, 2009). UDV is a non-invasive method of measuring velocity profiles (Asher, 1983), which is very useful in industrial applications. It utilizes pulsed ultrasonic echography together with the detection of the instantaneous frequency of the detected echo to obtain spatial information, and Doppler shift frequency. The latter provides the magnitude and direction of the velocity vector (Takeda, 1991). Compared to the conventional Doppler anemometry, and particle image velocimetry, UDV offers the following benefits (Takeda, 1986,1995; Williams, 1986; McClements, 1990): (i) more efficient flow mapping, (ii) applicability to opaque liquids, and (iii) the recording of the spatio-temporal velocity.

Figure 3 shows a comparison of the velocity data (axial and radial velocities) from the UDV measurements with the velocities computed using CFD for the Scaba 6SRGT impeller in the mixing of xanthan gum solution, which is an opaque shear-thinning fluid possessing yield stress (Pakzad et al., 2008b). It is observed that the CFD calculations pick up the features of the flow field, and the computed velocities agree well with the measured data.

4. Estimation of the cavern size

As mentioned earlier, the mixing of shear-thinning fluids with yield stress results in the formation of a well-mixed region called cavern around the impeller, and regions of stagnant or slow moving fluids elsewhere in the vessel.

The term cavern was introduced by Wichterle and Wein (1975) in the investigation of mixing of extremely shear thinning suspensions of finely divided particulate solids.

Solomon et al. (1981) modeled a spherical cavern assuming that the power dissipated by the impeller is transmitted through the fluid to the cavern wall, the shear stress at the cavern
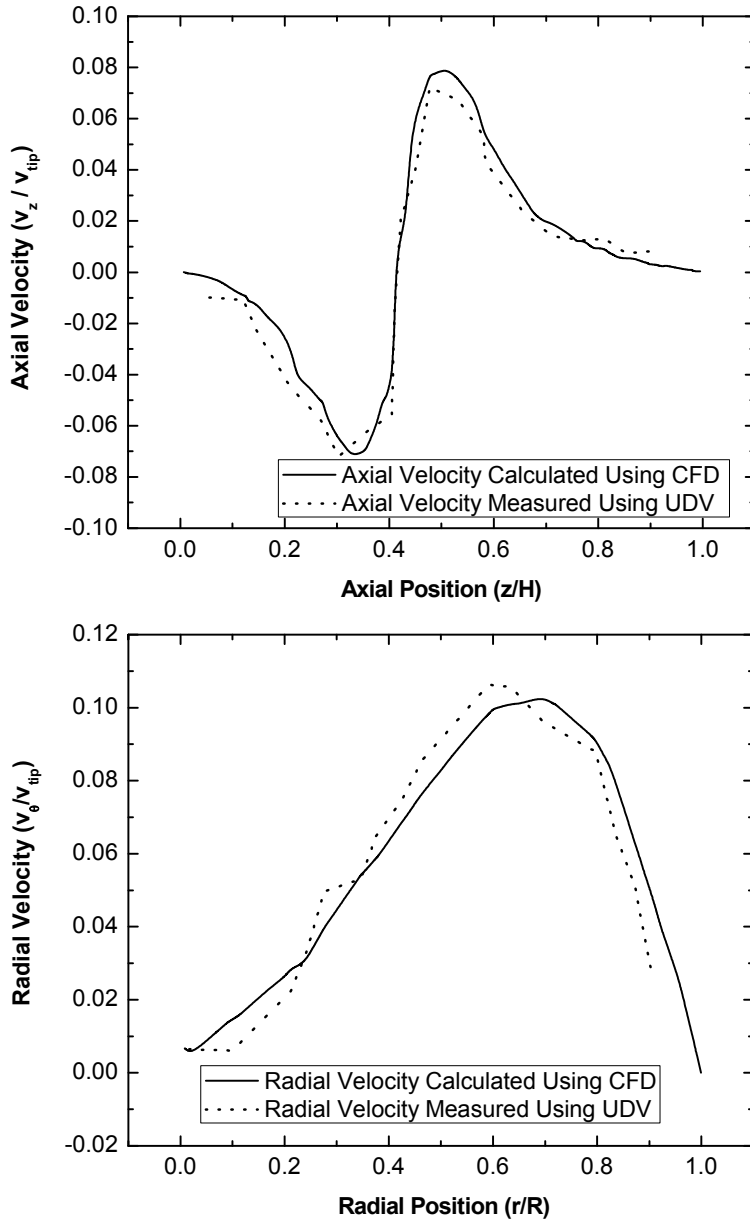

Fig. 3. (a) axial and (b) radial velocity profiles generated by the Scaba 6SRGT impeller at Re = 80.9

boundary equals the fluid yield stress, and the predominant motion of the fluid within the cavern is tangential. Elson et al. (1986, 1988) modified that for a more appropriate cylindrical cavern. A cylindrical cavern model was also proposed by Hirata & Aoshima (1994,1996). Amanullah et al. (1998) developed a mathematical model for a torus-shaped cavern. This model considers the total momentum imparted by the impeller as the sum of both tangential and axial shear components transported to the cavern boundary by the pumping action of the impeller. Wilkens et al. (2005) empirically developed an elliptical torus model neglecting the axial force to predict the cavern diameter and height, and using the yield stress of the fluid to define the cavern boundary. Table 2 lists these cavern models.

Model	Reference
$\left(\dfrac{D_c}{D}\right)^2 \propto \dfrac{\rho N^2 D^2}{\tau_y}$	Witchterle and Wein (1975, 1981)
$\left(\dfrac{D_c}{D}\right)^3 = \left(\dfrac{4P_0}{\pi^3}\right)\left(\dfrac{\rho N^2 D^2}{\tau_y}\right) = \dfrac{4}{\pi^3} P_0 \text{Re}_y$	Solomon et al. (1981)
$\left(\dfrac{D_c}{D}\right)^3 = \left(\dfrac{1.36 P_o}{\pi^2}\right)\left(\dfrac{\rho N^2 D^2}{\tau_y}\right) = \dfrac{1.36}{\pi^2} P_o \,\text{Re}_y$	Elson et al. (1986)
$\left(\dfrac{D_c}{D}\right)^3 = \dfrac{P_0 \text{Re}_y}{\left(H_c / D_c + 1/3\right)\pi^2}$	Elson (1988)
$\left(\dfrac{D_c}{D}\right)^3 = \left(\dfrac{4\alpha^2 P_0}{\pi}\right)\left(\dfrac{\text{Re}_y{}^2}{\text{Re}}\right)\left(\dfrac{H_c}{D_c}\right)$	Hirata & Aoshima (1995, 1996)
$\left(\dfrac{D_c}{D}\right)^2 = \dfrac{1}{\pi}\left(\dfrac{\rho N^2 D^2}{\tau_y}\right)\sqrt{N_f^2 + \left(\dfrac{4P_0}{3\pi}\right)^2}$	Amanullah et al. (1998)
$D_c = \alpha\left(\dfrac{P_0 N^2 D^5}{2\pi}\right)^{1/3}$, $H_c = \beta\left(\dfrac{P_0 N^2 D^5}{2\pi}\right)^{1/3}$	Wilkens et al. (2005)

Table 2. Various models proposed for cavern size

The contours of velocity magnitude generated CFD simulations can be used to analyze the formation of cavern around the impeller (Pakzad et al., 2008a; Saeed et al., 2008; Pakzad et al, 2008b; Ein-Mozaffari & Upreti, 2009). The boundary velocity for the cavern is considered to be $0.01v_{\text{tip}}$, where v_{tip} is the impeller tip velocity. Thus, the fluid velocity is greater than $0.01v_{\text{tip}}$ within the cavern, and less than $0.01v_{\text{tip}}$ in the surrounding. Pakzad et al. (2008a) employed CFD to measure the size of the cavern generated around the Scaba 6SRGT impeller in the mixing of xanthan gum solution. Figure 4 shows the formation of cavern around the Scaba 6SRGT impeller for Re equal to 30 and 110 (Pakzad, 2007). To validate the CFD results for the cavern size, Pakzad et al. (2008a) used the Electrical Resistance Tomography (ERT) to measure the cavern diameter. ERT is a non-intrusive technique to interrogate the three dimensional concentration fields inside the mixing tanks. It enables effective measurements of the homogeneity and flow pattern inside the mixing vessel.
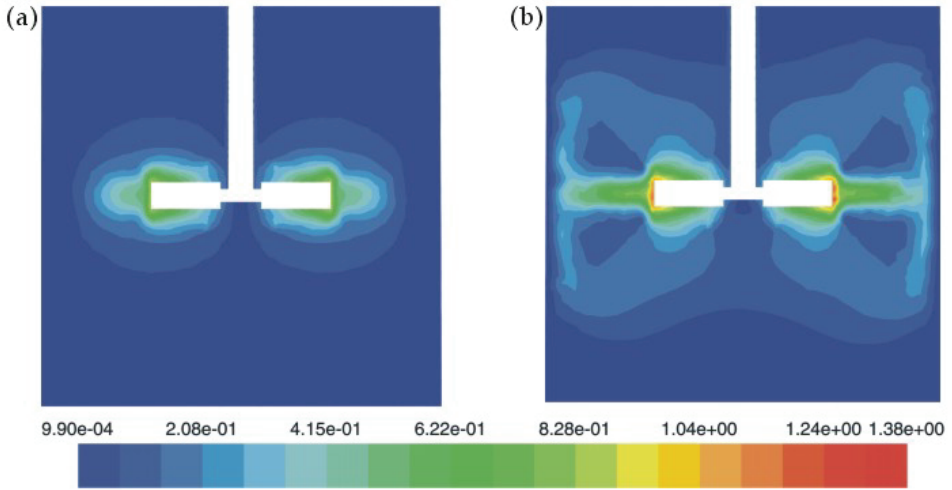
Fig. 4. Cavern formation at (a) Re = 30 and (b) Re = 110 around the Scaba 6SRGT impeller in the mixing of xanthan gum solution

Based on the CFD and ERT results, it was observed that the cavern can be represented by a right circular cylinder. Figure 5 shows the dimensionless cavern diameter (D_c/D) versus dimensionless $P_0\mathrm{Re}_y$ for the Scaba 6SRGT impeller. These results show good agreement between calculated cavern diameter using CFD, and the experimentally counterpart
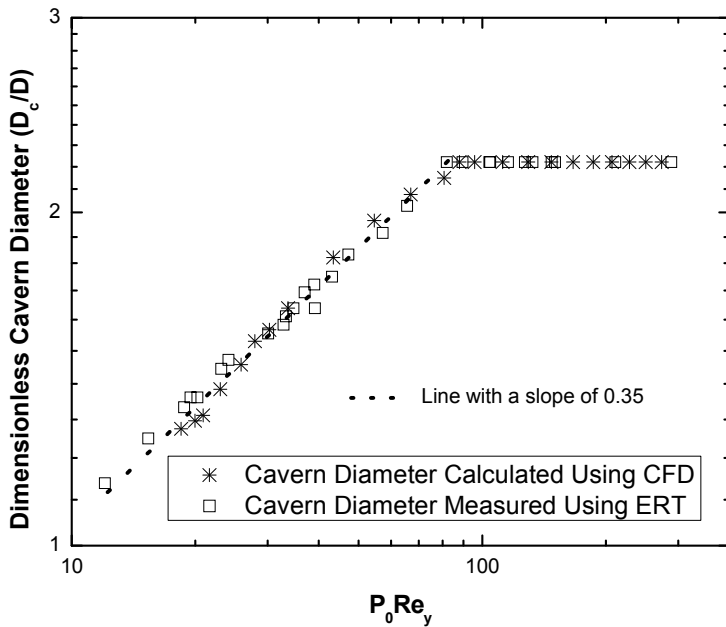

Fig. 5. Cavern diameter as a function of $P_0\mathrm{Re}_y$ for the Scaba 6SRGT impeller

determined using ERT. It can be seen that for P_0Re_y greater than 80, the cavern reached the vessel walls ($D_c = T$) and D_c/D remained constant. The slope of the line was 0.35 for P_0Re_y less than 80.

The cylindrical model (Elson, 1988) predicts a theoretical slope of 0.33 from a log-log plot of D_c/D versus P_0Re_y (see Table 2). Thus, the CFD predictions show a good agreement with the Elson model as well. Further, Pakzad et al. (2008a) found that the ratio of the cavern height H_c to D_c stayed at 0.48 until the cavern reached the tank wall with $D_c = T$. After that happened, the height of the cavern increased with the impeller speed such that

$$\frac{H_C}{D_C} \propto N^{0.58} \tag{17}$$

This result is in good agreement with that reported by Galindo & Nienow (1993) for the Scaba 6SRGT impeller.

In addition, Ein-Mozaffari & Upreti (2009) also used CFD simulations to analyze the shape and the size of cavern generated around three axial-flow impellers: marine propeller, pitched blade turbine, and Lightnin A310 impeller.

Their CFD results were in good agreement with those reported by Galindo & Nienow (1992) for the axial-flow Lightnin A315 impeller.

5. Calculation of impeller flow number

The rotary motion of the impeller has a pumping effect: the liquid is drawn towards the impeller and then pumped away from it, with the outgoing flow having a predominant radial, axial, or an intermediate direction. The high-velocity outgoing flow entrains the neighboring liquid into motion, thus the overall circulating liquid combines both the pumped out and the entrained liquid.

In order to assess the pumping capacity of the impeller at different operating conditions, the impeller flow number and the circulation number must be evaluated. Saeed et al. (2009) used CFD to calculate the flow and circulation numbers for three axial-flow impellers in the mixing of a shear-thinning fluid with yield stress. The pumping flowrate encompassing the impeller swept volume is given by (Mishra et al., 1998)

$$Q_P = 2\pi \int_0^{D/2} \left(r v_z \right)\Big|_{z_1} \mathrm{d}r + \pi D \int_{z_1}^{z_2} v_r \big|_{D/2} \mathrm{d}z \tag{18}$$

where D, v_r and v_z respectively are impeller diameter, radial velocity, and axial velocity; and z_1 and z_2 are the boundaries of the impeller-swept volume in the axial direction. The second term in Equation (18) is negligible for the axial flow impellers (Patwardhan & Joshi, 1999; Kumaresan & Joshi, 2006). Thus, the flow number (Fl) can be estimated for axial flow impellers from the following equation using Q_P:

$$\mathrm{Fl} = \frac{Q_P}{ND^3} = \frac{2\pi}{ND^3} \int_0^{D/2} r v_z \mathrm{d}r \tag{19}$$

Saeed et al. (2008) have utilized the axial velocities obtained using CFD to calculate the flow numbers for Lightnin A100, A200, and A310 impellers (Table 3).

	Impeller		
Parameter	A100	A200	A310
Power Number	0.66	1.16	0.40
Flow Number	0.42	0.47	0.37
Circulation Number	0.89	0.92	0.77
Pumping Efficiency	0.636	0.405	0.925
Circulation Efficiency	1.348	0.793	2.139

Table 3. Specifications of three axial-flow impellers (Saeed et al. 2008)

It must be mentioned that the flow numbers shown in Table 3 for xanthan gum solution are less than those reported in literature for water. Other researchers have reported that the impeller flow number is a function of the rheologial properties of the fluid (e.g. viscosity and yield stress). Jaworski & Nienow (1993) found that the impeller flow number for carboxymethyl cellulose solutions was lower than that for water, and Mavros et al. (1996) showed that as liquid viscosity increased the impeller flow rate decreased. Using measured velocity profiles across the impeller, Ein-Mozaffari et al. (2007a) found that the pulp suspension yield stress increased (by increasing fibre mass concentration, or fibre length) with the decrease in Fl.

The circulation number for an axial flow impeller is defined as follows (Ranade & Dommeti, 1996; Aubin et al., 2001):

$$\text{Fl}_c = \frac{Q_c}{ND^3} = \frac{2\pi}{ND^3} \int_0^{r|_{v_z}} \left(r v_z \right)\big|_{z_1} \, dr \tag{20}$$

where Q_c is overall liquid circulation generated in impeller swept volume and includes flow entrained by impeller discharge, and $r\big|_{v_z}$ is the radius where the axial flow velocity reverses from downward to upward direction in the downward pumping impellers. Table 3 shows the circulation numbers calculated using CFD for three axial flow impellers in the mixing of xanthan gum solution (Saeed, 2007; Saeed et al., 2008).

The impeller pumping efficiency (η_p) and circulation efficiency (η_c) can be used to compare the performances of the different impellers in the mixing of shear-thinning fluids possessing yield stress (Mishra et al, 1998; Aubin et al., 2001):

$$\eta_p = \text{Fl} / P_0 \tag{21}$$

$$\eta_c = \text{Fl}_c / P_0 \tag{22}$$

The pumping and circulation efficiencies computed by CFD for the Lightnin A100, A200, and A310 impellers in the mixing of the xanthan gum solution are listed in Table 3 (Saeed, 2007). These results show that the A310 impeller is superior to the rest.

Pakzad et al. (2008b) employed CFD to measure the impeller flow number as a function of Reynolds number for a radial-flow impeller used for the mixing of a shear-thinning fluid with yield stress. For a radial-flow impeller, the first term in Equation (18) is negligible. Thus, the impeller flow number for a radial-flow impeller is defined by:

$$\text{Fl} = \frac{Q_P}{ND^3} = \frac{\pi}{ND^2} \int_{z_1}^{z_2} v_r\big|_{D/2} \, dz \tag{23}$$

Figure 6 depicts the impeller flow number versus Re for the radial-flow Scaba 6SRGT impeller utilized for the mixing of the xanthan gum solution (Pakzad et al., 2008b).

6. Analysis of mixing time

Mixing time is a key variable, which provides a powerful way to evaluate mixing effectiveness, and compare mixing systems (Paul et al, 2004). It is defined as the time elapsed between the instant when a tracer of similar rheological properties as the bulk fluid is added, and the instant at which the vessel contents attain a specified degree of uniformity (Harnby et al., 1997); usually the expected equilibrium tracer concentration.

If there is no tracer initially present in the vessel, then the mixing time, t_m, can be defined as the time between tracer addition to the time when

$$\frac{|C - C_\infty|}{C_\infty} = m \tag{24}$$

where C is the tracer concentration, C_∞ is its equilibrium value, and m is the maximum acceptable deviation from homogeneous conditions (Ihejirica & Ein-Mozaffari, 2007).
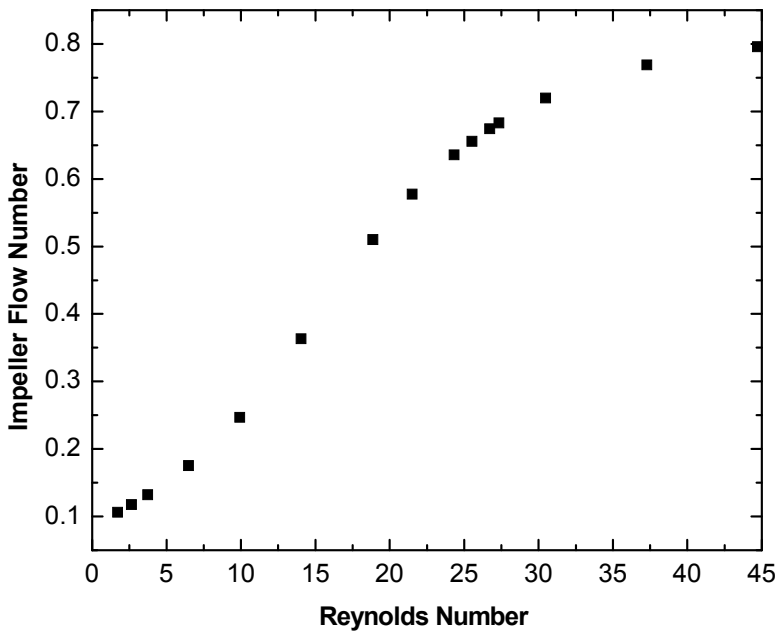

Fig. 6. Impeller flow number as a function of Re for the mixing of the xanthan gum solution with the Scaba 6SRGT impeller

The mixing time can be obtained through experiments as well as CFD. Some of the experimental methods are not applicable for the opaque fluids, and the probe techniques have the disadvantage of affecting the flow pattern inside the tank. The advantage of CFD is that it provides comprehensive data not easily obtained from the experimental techniques.

To simulate the mixing times after the convergence of the flow field through CFD, the unsteady state transport of an inert tracer superimposed on the calculated flow field is monitored until complete homogenization is achieved. Assuming tracer distribution by convection and diffusion, the unsteady distribution of the tracer is determined by solving the species transport equation (Ein-Mozaffari & Upreti, 2009)

$$\frac{\partial}{\partial t}(\rho m_t) = -\nabla \cdot (\rho v m_t) + \nabla \cdot (\Gamma \nabla m_t) \tag{25}$$

where m_t is the mass fraction of the tracer species, v is the mean velocity vector, and Γ is the molecular diffusivity. Γ has negligible effect on the tracer distribution possibly because the insignificant contribution of molecular diffusion to the overall tracer dispersion (Montante et al., 2005). Some researchers also find that the effect of the molecular diffusivity is negligible in the mixing of non-Newtonian fluids in the laminar regime (Saeed et al., 2007; Ihejirika & Ein-Mozaffari, 2007; Ein-Mozaffari & Upreti, 2009).

Pakzad (2007) used CFD to predict the mixing time for the agitation of the shear-thinning fluid possessing yield stress with a Scaba 6SRGT impeller. The tracer concentration was monitored at four locations as depicted in Figure 7. The tracer concentration C was normalized using the tracer concentration at time equal to infinity (C_∞), which represents a perfectly mixed condition, to give a normalized tracer concentration (C/C_∞). The mixing system was considered homogeneous when the normalized tracer concentrations at all four monitoring points were equal to one. The mixing time was defined as the time required for the normalized tracer concentrations at all four monitoring points to reach 95% of the steady state value (Figure 8).
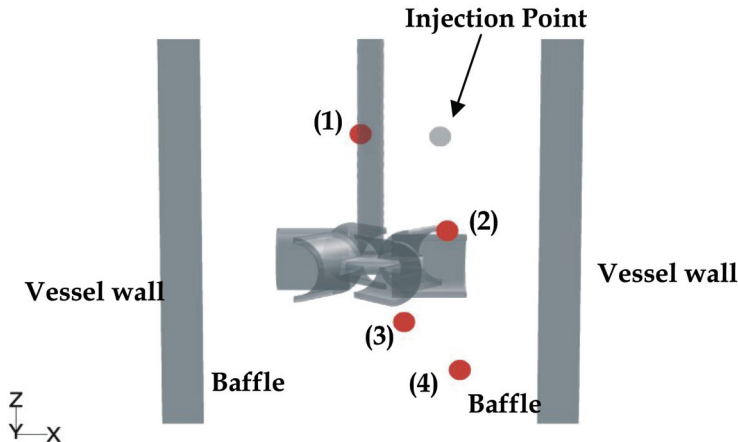

Fig. 7. Injection point and four monitoring locations (1, 2, 3, and 4) used to predict t_m

To evaluate the accuracy of this technique, Pakzad (2007) compared the mixing time values computed by the CFD model with those measured through electrical resistance tomography (ERT) for xanthan gum solution. Figure 9 shows that although the CFD model underpredicted the mixing time for the shear-thinning fluid possessing yield stress, there was a reasonable agreement between the CFD and ERT results.
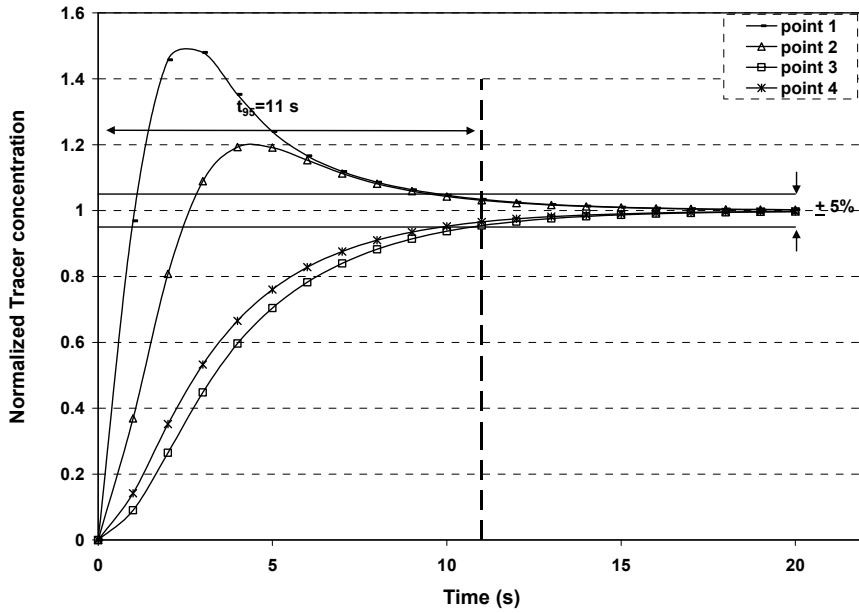
Fig. 8. Normalized tracer concentration versus time for four monitoring points
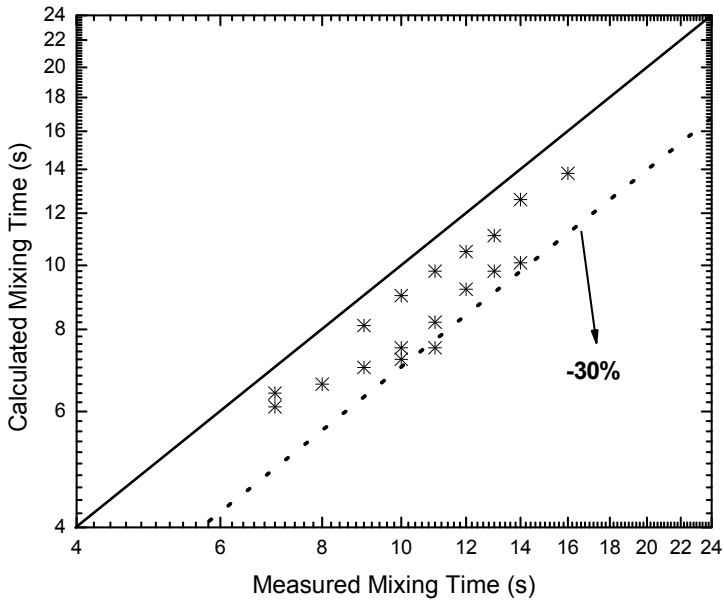

Fig. 9. Calculated versus measured mixing time for the xanthan gum solution agitated with a Scaba 6SRGT impeller

Ihejirika & Ein-Mozaffari (2007) utilized CFD technique to investigate the effect of impeller pumping direction on the mixing performance for a pseudoplastic fluid with yield stress agitated in a cylindrical tank equipped with a helical ribbon impeller. To achieve this goal, they used the following two parameters: (i) the dimensionless mixing time Nt_m, and (ii) the performance rating given by $Pt_m^2 / (\eta D^3)$. While Nt_m represents the number of revolutions of the agitator required to achieve a specified level of homogeneity (Kappel, 1979; Delaplace et al., 2000), $Pt_m^2 / (\eta D^3)$ is a function of the mixing time Reynolds number given by $D^2 \rho / (\eta t_m)$ (Tatterson, 1991).

The authors showed that Nt_m was a constant for a specific geometry of close clearance impellers such as helical ribbons in the laminar flow regime. The average Nt_m value for the helical ribbon pumping upwards was 27 as compared to an average value of 33 in the downward pumping mode. From the definition of Nt_m, it is clear that in pumping downwards, the impeller requires more rotations to achieve the desired level of uniformity. This translates into longer mixing times.

The performance rating $Pt_m^2 / (\eta D^3)$ represents energy divided by the volumetric performance of the mixing equipment. It allows the decision as to which impeller exhibits the lowest specific power consumption in mixing a given fluid with required mixing intensity in a vessel of given volume. Figure 10 depicts the performance rating versus the mixing time Reynolds number (Ihejirica & Ein-Mozaffari, 2007) obtained for a helical ribbon impeller used for the agitation of xanthan gum solution. It can be seen that the helical ribbon impeller pumping upwards is the more efficient mode of operation because this pumping direction gives lower values of $Pt_m^2 / (\eta D^3)$ in the entire operating flow regime.
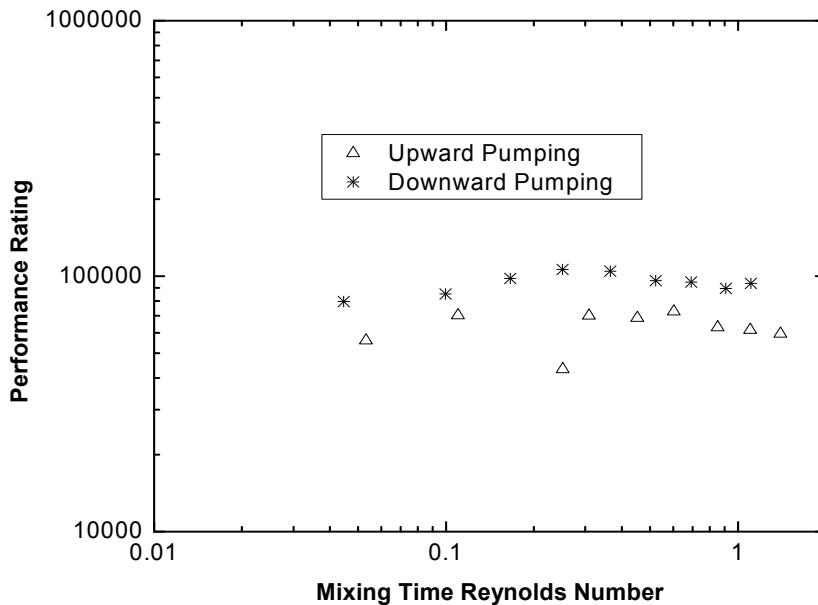

Fig. 10. Performance rating versus mixing time Reynolds number for helical ribbon impeller

Saeed et al. (2007) employed the CFD technique to estimate the mixing time in the mixing of the pulp suspension with a side-entering Lightnin A310 impeller in a rectangular chest. Pulp suspension is a shear-thinning fluid possessing yield stress whose rheology was approximated using Herschel-Bulkley model. The authors showed that the mixing time computed from CFD simulation was the following function of the impeller momentum flux (Figure 11):

$$t_m = 17.21(N^2 D^4)^{-1.03} \tag{26}$$

The impeller momentum flux, which is proportional to $N^2 D^4$, was introduced by Fox & Gex (1956) for mixing time correlation and used by Yackel (1990) for designing agitated pulp stock chests. This parameter was correlated with the mixing time (t_m) of pulp suspension by Ein-Mozaffari et al. (2003).
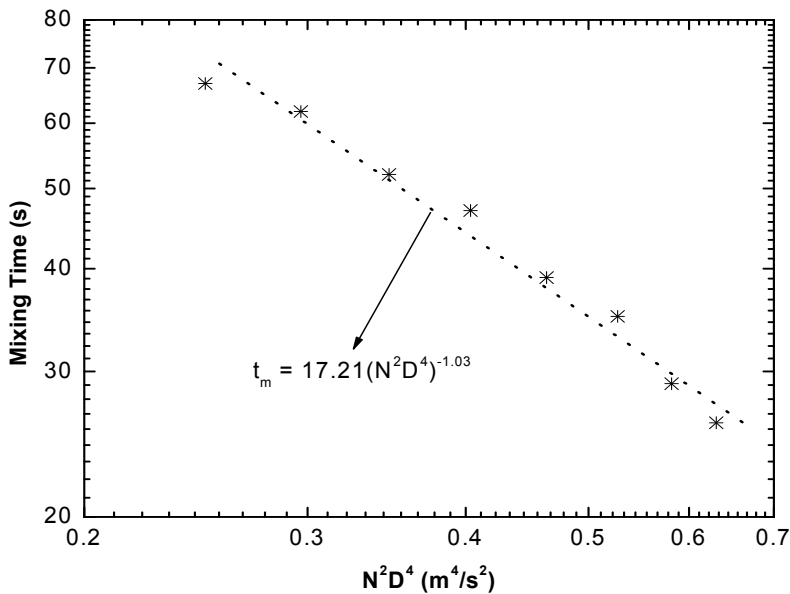

Fig. 11. Mixing time as a function of N^2D^4 for pulp suspension agitated in a rectangular chest equipped with a side-entering Lightnin A310 impeller

Ein-Mozaffari & Upreti (2009) utilized CFD to evaluate the performances of three axial-flow impellers (pitched blade turbine (PBT), marine propeller, and Lightnin A310) in the mixing of shear-thinning fluids with yield stress. To achieve this goal, they calculated mixing time and impeller specific power (power/mass) through CFD. Figure 12 illustrates mixing time versus specific power for these three impellers used for the mixing of xanthan gum solution. It can be seen that for a given power input, the A310 impeller achieved homogenization in the shortest time. The results also show that the pitched blade turbine (PBT) gives longer mixing times compared to the marine propeller, and A310 impeller at a specific power input. Thus, in order to minimize the mixing time, an impeller with a large pumping efficiency such as the A310 impeller should be chosen for the mixing of shear-thinning fluids with yield stress.
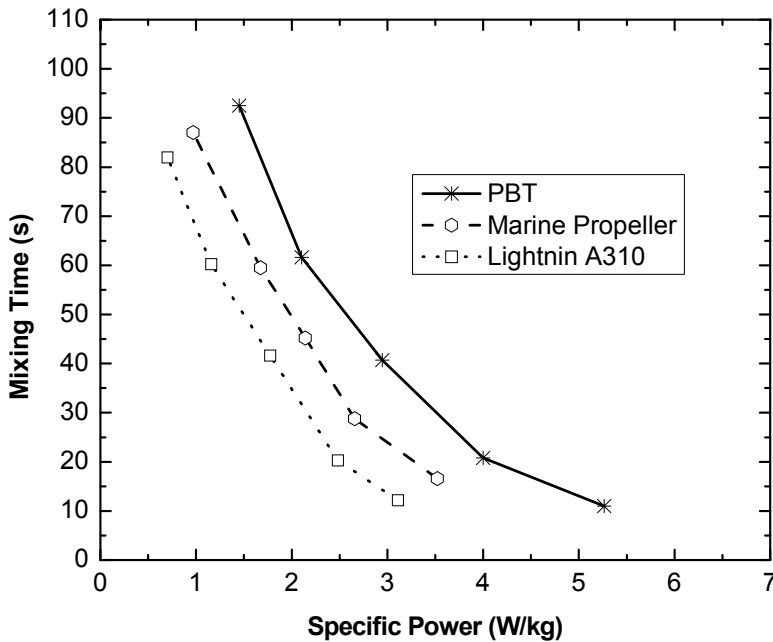
Fig. 12. Mixing time versus specific power for three axial-flow impellers used for the agitation of xanthan gum solution

7. Analysis of the continuous-flow mixing of shear-thinning fluids possessing yield stress

Continuous mixing has numerous advantages over the batch mixing since continuous operations allow high production rates, enhanced process control, and reduce operation times by eliminating pump-out, filling and between-cycle cleaning. Continuous-flow mixing is a vital component to many processes including polymerization, fermentation, waste water treatment, and pulp and paper manufacturing. Shear thinning fluids with yield stress are commonly encountered in the aforementioned processes (Saeed & Ein-Mozaffari, 2008; Saeed et al., 2008).

Continuous-flow mixers have traditionally been designed based upon ideal flow assumption (Levenspiel, 1998). However, the complex rheology displayed by the non-Newtonian fluids can create considerable deviation from ideal mixing. Dynamic tests conducted on those mixing vessels show that the non-ideal flow such as channelling, recirculation, and dead zones significantly affect the performance of the continuous mixing processes (Ein-Mozaffari et al., 2003b, 2004a, and 2004b). A dynamic model incorporating the effect of these non-ideal flows was proposed by Ein-Mozaffari (2002) for continuous-flow mixing processes. This model allows for two parallel flow paths through the mixing vessel:

i.   the channelling zone comprising the first order transfer function with a delay, and

ii.   the mixing zone comprising the first order transfer function with a delay, and feedback for recirculation (Figure 13).
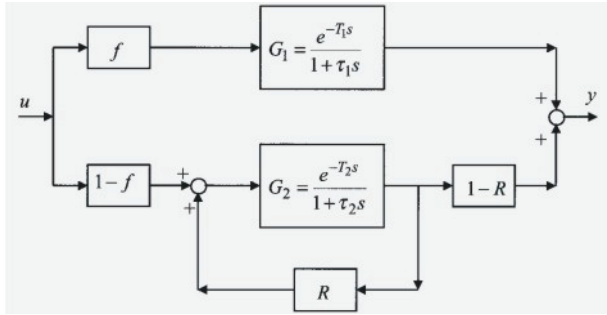
Fig. 13. Block diagram of the continuous-flow mixing processes

The combined transfer function for flow paths in a continuous time domain can be expressed mathematically as follows:

$$G = \frac{f\, e^{-T_1 s}}{1 + \tau_1 s} + \frac{(1-f)\,(1-R)\, e^{-T_2 s}\left(1 + \tau_2 s\right)^{-1}}{1 - R\, e^{T_2 s}\left(1 + \tau_2 s\right)^{-1}} \tag{27}$$

where G is the transfer function of the vessel, f is the portion of the fluid channelled in the mixing tank, and R is the portion of the fluid recirculated within the mixing vessel. τ_1 and τ_2 are the time constants for the channelling and mixing zones. T_1 and T_2 are the time delays for the channelling and agitated zone, respectively.

The identification experiment is performed through exciting the system by the frequency-modulated random binary signal and observing the input and output signals over a time interval (Ein-Mozaffari, 2003b). By measuring the input-output signals of the mixing vessel, the dynamic model parameters can be estimated using a numerical method developed by Kammer et al. (2005). Two distinct stages were used for the identification in this method: an efficient but less accurate least squares minimization for the optimal delays followed by an accurate gradient search for all parameters. Although this algorithm did not ensure convergence to the global minimum, a Monte Carlo simulation showed very encouraging results. Later on, a hybrid genetic algorithm bridged that gap and identified the mixing parameters with high accuracies (Upreti & Ein-Mozaffari, 2006; Patel et al., 2008).

Since the dynamic tests conducted on both lab-scale and industrial-scale mixing vessels are costly and time-consuming, Saeed (2007) and Saeed et al. (2008) utilized CFD to study the dynamic behavior of the continuous-flow mixing processes. Fluent was used to simulate xanthan gum flow within the continuous mixing vessel under steady state. Boundary conditions imposed on the system included: (i) non-slip at the vessel wall and baffles, (ii) zero normal velocity at the free surface, (iii) inflow boundary condition for vessel inlet, defining inlet velocity from the volumetric flow rate of the feed, i.e. $v = 4Q / (\pi d^2)$ where Q is volumetric flow rate, and d is the inlet diameter of the pipe; and (iv) outflow boundary condition for vessel outlet, implying zero normal diffusive flux for all flow variables (Versteeg & Malalasekera, 2007).

To simulate the dynamic test after the convergence of the flow field through CFD, a user defined function (UDF), written in C programming language, was linked to Fluent solver (Saeed, 2007). The UDF defines the time at which the tracer was continuously injected to the mixing vessel. The UDF was linked to the inlet as a boundary condition that specifies the

tracer concentration in the inlet stream. Outlet concentration was recorded for comparison with experimental data later. Mass fraction of tracer in UDF was set to the values analogous to the conductivity of the random binary excitation signal used in the experimental work (Saeed et al., 2008). In order to evaluate the CFD ability to predict the dynamic behavior of the continuous-flow mixers, experimental and CFD input-output conductivity curves for tracer injections were compared against each other in Figure 14 (Saeed, 2007; Saeed et al., 2008).
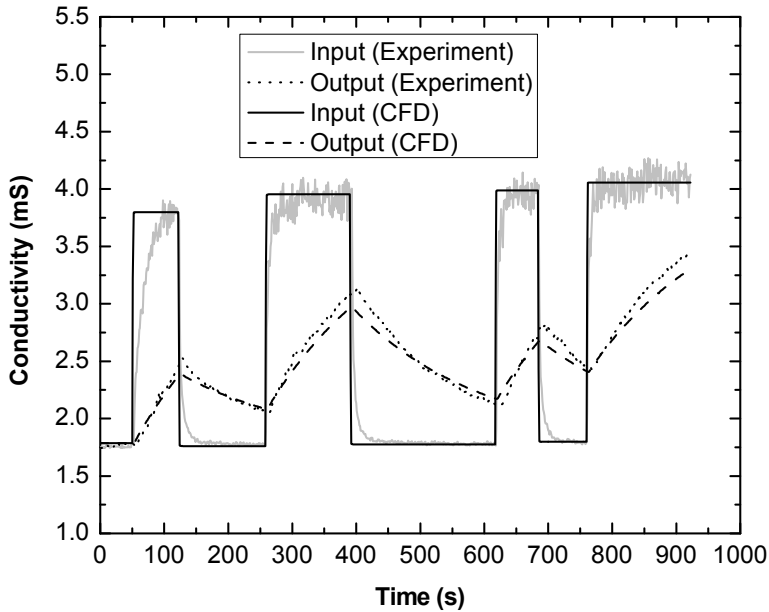

Fig. 14. Input and output signals in flow situations containing insignificant channelling

The noise associated with measured input signals was excluded from input signals used in CFD simulations. The output response predicted by CFD demonstrated good agreement with the experimental response. However, the authors observed that the signal output computed using CFD deviated from measured output in flow situations containing significant channelling (Figure 15). Similar observations were reported for the mixing of pulp suspension in a rectangular chest equipped with a side-entering impeller (Ford et al., 2006).

Two parameters have been widely used to quantify the performance of the continuous-flow mixing process: (i) the extent of channelling f in the vessel, and (ii) and the ratio of the fully-mixed volume V_{fm} to the total volume V_t of the fluid in the mixing tank (Ein-Mozaffari et al., 2004a, 2004b, 2005, 2007b). The fraction of fully-mixed volume is given by

$$\frac{V_{fm}}{V_t} = \frac{Q\tau_2\left(1-f\right)}{V_t} \tag{28}$$

where Q is the solution flow rate through the mixing vessel. Table 4 compares CFD and experimental results for the extent of channelling and fully-mixed volume at two different
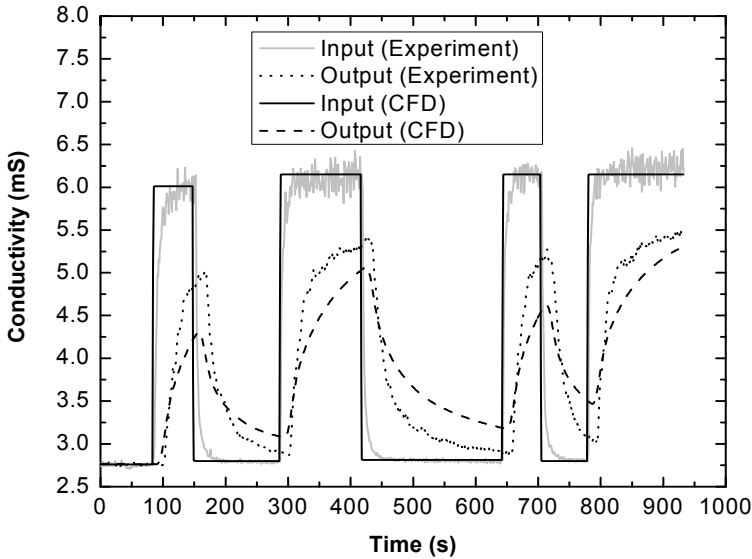
Fig. 15. Input – output signals in flow situations containing significant channeling

xanthan gum concentrations (Saeed, 2007; Saeed et al., 2008). It can be seen that the CFD results are in a good agreement with the experimentally determined values.

Saeed et al. (2008) used CFD to investigate the effect of impeller type on the dynamic behavior of the continuous-flow mixing of xanthan gum solution. Table 5 summarizes the extent of channelling and fully mixed volume for three axial-flow impellers (Lightnin A100, A200, and A310). A comparison of CFD and experimental data in this table reveals that the A310 impeller was able to reduce channelling and increase fully-mixed volume in the vessel. They concluded that in order to minimize the extent of channelling and dead volume in a continuous-flow mixer, an impeller with a large pumping and circulation efficiency such as A310 should be chosen.

Parameter	0.5% xanthan gum		1.5% xanthan gum	
	Experiment	CFD	Experiment	CFD
f	0.09	0.07	0.18	0.15
V_{fm} / V_t	0.91	0.94	0.83	0.87

Table 4. Extent of channelling and fully-mixed volume at two different xanthan gum concentrations

Impeller	f		V_{fm} / V_t	
	Experiment	CFD	Experiment	CFD
A100	0.17	0.13	0.91	0.98
A200	0.19	0.15	0.88	0.93
A310	0.15	0.10	0.97	0.98

Table 5. Extent of channeling and fully-mixed volume for three axial-flow impellers

Ein-Mozaffari et al.(2005), Saeed & Ein-Mozaffari (2008), and Saeed et al. (2008) explored the effect of cavern formation around the impeller on the dynamic behavior of the continuous-flow mixing of the shear-thinning fluids possessing yield stress. They found that the size of the cavern generated around the impeller has a significant effect on the extent of non-ideal flow in continuous mixing of fluids with yield stress. As the impeller speed increases, the cavern surface moves towards the tank wall and the fluid surface within the mixing vessel.When the cavern does not reach the vessel wall and fluid surface, a high percentage of the feed stream will be channelled easily to the exit without being entrained in the impeller flow. Thus, the continuous-flow mixing system is prone to a high level of non-ideal flow.

8. Conclusion

This chapter presented the application of Computational Fluid Dynamics (CFD) along with stat-of-the-art experimental techniques of Ultrasonic Doppler Velocimetry (UDV), and Electrical Resistance Tomography (ERT) to capture the mixing of shear-thinning fluids with yield stress. The mathematical underpinnings of the CFD approach, and the experimental methods were elaborated. To demonstrate the utility of CFD, we included the results of relevant investigations juxtaposing the CFD simulations against the experimental tests of mixing the shear thinning fluids.

9. References

Amanullah, A.; Hjorth, S.A. & Nienow, A.W. (1998). A new mathematical model to predict cavern diameters in highly shear thinning, power law liquids using axial flow impellers. *Chem. Eng. Sci.*, Vol. 53, No. 3, 455-469.

Armenante, P.M.; Luo, C.; Chou, C.C.; Fort, I. & Medek, J. (1997). Velocity profiles in a closed, unbaffled vessel: comparison between experimental ldv data and numerical cfd prediction. *Chem. Eng. Sci.*, Vol. 52, No. 20, 3483-3492.

Asher, R.C. (1983). Ultrasonic sensors in the chemical and process industries. *J. Phys. E: Sci. Instrum.*, Vol. 16, No. 10, 959-963.

Aubin, J.; Mavros, P.; Fletcher, D.F.; Bertrand, J. & Xuereb, C. (2001). Effect of axial agitator configuration (up-pumping, down-pumping, reverse-rotation) on flow patterns generated in stirred vessels. *Chem. Eng. Res. Des.*, Vol. 79, No. 8, 845-856.

Aubin, J.; Fletcher, D.F. & Xuereb, C. (2004). Modeling turbulent flow in stirred tanks with cfd: the influence of the modeling approach, turbulent model and numerical scheme. *J. Exp. Thermal Fluid Sci.*, Vol. 28, No. 5, 431-445.

Bird, R.B.; Stewart, W. E. & Lightfoot E.N. (2002). *Transport Phenomena*. John Wiley & Sons, New York.

Brucato, A.; Ciofalo, M.; Grisafi, F. & Micale, G. (1998). Numerical prediction of flow fields in baffled vessels: a comparison of alternative modeling approaches. *Chem. Eng. Sci.*, Vol. 53, No. 21, 3653-3684.

Bujalski, W.; Jaworski, Z. & Nienow, A.W. (2002). CFD study of homogenization with dual rushton turbines - comparison with experimental results: Part II: The multiple reference frame, *Chem. Eng. Res. Des.*, Vol. 80, No. 1, 97-104.

Delaplace, G.; Leuliet, J.C. & Relandeau, V. (2000). Circulation and mixing times for helical ribbon impellers: Review and experiments, *Exp. Fluids*, Vol. 28, 170-182.

Ein-Mozaffari, F. (2002). *Macroscale Mixing and Dynamic Behavior of Agitated Pulp Stock Chests*. Ph.D. Thesis, University of British Columbia, Vancouver.

Ein-Mozaffari, F.; Dumont, G.A. & Bennington, C.P.J. (2003a). Performance and design of agitated pulp stock chests. *Appita J.*, Vol. 56, No. 2, 127-133.

Ein-Mozaffari, F.; Kammer, L.C.; Dumont, G.A. & Bennington, C.P.J. (2003b). Dynamic modeling of agitated pulp stock chests. *TAPPI J.*, Vol. 2, No. 9, 13-17.

Ein-Mozaffari, F.; Kammer, L.C.; Dumont G.A. & Bennington, C.P.J. (2004a). The effect of operating conditions and design parameters on the dynamic behavior of agitated pulp stock chests. *Can. J. Chem. Eng.*, Vol. 82, No. 1, 154-161.

Ein-Mozaffari, F.; Bennington C.P.J. & Dumont, G.A. (2004b). Dynamic mixing in industrial agitated stock chests. *J. Pulp Paper Can.*, Vo. 105, No. 5, 41-45.

Ein-Mozaffari, F; Bennington C.P.J. & Dumont, G.A. (2005). Suspension yield stress and the dynamic response of agitated pulp chests. *Chem. Eng. Sci.*, Vol. 60, No. 8, 2399-2408.

Ein-Mozaffari, F.; Bennington, C.P.J.; Dumont, G.A. & Buckingham, D. (2007a). Measuring flow velocity in pulp suspension mixing using ultrasonic doppler velocimetry. *Chem. Eng. Res. Des.*, No. 85, No. A5, 591-597.

Ein-Mozaffari, F.; Bennington, C.P.J. & Dumont, G.A. (2007b). Optimization of rectangular pulp stock mixing chest dimensions using dynamic tests. *TAPPI J.*, Vol. 6, No. 2, 24-30.

Ein-Mozaffari, F. & Upreti, S.R. (2009). using ultrasonic doppler velocimetry and CFD modeling to investigate the mixing of non-newtonian fluids possessing yield stress. *Chem. Eng. Res. Des.*, Vo. 87, No. 4, 515-523.

Elson, T.P. (1988). Mixing of fluids possessing a yield stress, *Proceedings of 6th European Conference on Mixing*, pp. 485-492, Pavia. Italy, 1988, AIDIC.

Elson, T.P.; Cheesman, D.J. & Nienow, A.W. (1986). X-Ray studies of cavern sizes and mixing performance with fluids possessing a yield stress. *Chem. Eng. Sci.*, Vol. 41, No.10, 2555-2562.

Ford, C.; Ein-Mozaffari, F.; Bennington, C.P.J. & Taghipour, F. (2006). simulation of mixing dynamics in agitated pulp stock chests using CFD. *AIChE J.*, Vol. 52, No. 10, 3562-3569.

Fox, E.A. & Gex, V.E. (1956). Single-phase blending of liquids. *AIChE J.*, Vol. 2, No. 4, 539-544.

Galindo, E. & Nienow, A.W. (1992). Mixing of highly viscous simulated xanthan fermentation broths with the lightnin a-315 impeller. *Biotechnol. Prog.*, Vol. 8, No. 3, 223-239.

Galindo, E. & Nienow, A.W. (1993). The performance of the Scaba 6SRGT agitator in the mixing of simulated xanthan gum broths. *Chem. Eng. Technol.*, Vol. 16, No. 2, 102-108.

Galindo, E.; Torrestiana, B. & García-Rejón, A. (1989). Rheological characterization of xanthan fermentation broths and their reconstituted solutions. *Bioproc. Eng.*, Vol. 4, 113-118.

Harnby, N.; Edwards, M.F. & Nienow, A.W. (1997). *Mixing in the Process Industries*, Butterworth-Heinemann, Boston.

Hirata, Y. & Aoshima, Y. (1994). Flow characteristics and power consumption in an agitated shear-thinning plastic fluid. *IChem. E. Symp.*, Vol. 136, 415-422.

Hirata, Y. & Aoshima, Y. (1996). Formation and growth of cavern in yield stress fluids agitated under baffled and non-Newtonian conditions. *Chem. Eng. Res. Des.*, Vol. 74, 438-444.

Ihejirika, I. & Ein-Mozaffari, F. (2007). Using CFD and ultrasonic velocimetry to study the mixing of pseudoplastic fluids with a helical ribbon impeller. *Chem. Eng. Tech.*, Vol. 30, No. 5, 606-614.

Jaworski, Z. & Nienow A.W. (1993). An LDA study of the hydrodynamics of caverns formed in a yield stress fluid agitated by a hydrofoil impeller. *Proceedings of CHISA 93*, paper H.6.2, Prague, 1993.

Jaworski, Z.; Dyster, K.N. & Nienow, A.W. (2001). The effect of size, location and pumping direction of pitched blades turbine impellers on flow patters: LDA measurements & CFD predictions. *Chem. Eng. Res. Des.*, Vol. 79, No. 8, 887-894.

Kammer, L.C.; Ein-Mozaffari, F.; Dumont, G.A. & Bennington, C.P.J. (2005). Identification of channellng and recirculation parameters of agitated pulp stock chests. *J. Process Control*, Vol. 15, No. 1, 31-38.

Kappel, M. (1979). Development and application of a method for measuring the mixture quality of miscible liquids: Application of the new method for highly viscous Newtonian liquids. *Int. Chem. Eng.*, Vol. 19, 571-590.

Kelly, W. & Gigas, B., (2003). Using CFD to predict the behavior of power law fluids near axial- flow impellers operating in the transitional flow regime. *Chem. Eng. Sci.*, Vol. 58, No. 10, 2141-2152.

Khopkar, A.R.; Mavros, P.; Ranade, V.V. & Bertrand, J. (2004). Simulation of flow generated by an axial flow impeller-bath and continuous operation. *Chem. Eng. Res Des.*, Vol. 82, No. 6, 737-751.

Khopkar, A.R.; Kasat, G.R.; Pandit, A.B. & Ranade, V.V. (2006). Computational fluid dynamics simulation of the solid suspension in a stirred slurry reactor. *Ind. Eng. Chem. Res.*, Vol. 45, No. 12, 4416-4428.

Kumaresan, T. & Joshi, J.B. (2006). Effect of impeller design on the flow pattern and mixing in stirred tanks, *Chem. Eng. J.*, Vol. 115, No. 3, 173-193.

Levenspiel, O., (1998). *Chemical Reaction Engineering*. John Wiley & Sons, New York.

Luo, J.Y.; Gosman, A.D.; Issa, R.I.; Middleton, J.C. & Fitzgerald, M.K. (1993). Full flow field computation of mixing in baffle stirred vessels. *Chem. Eng. Res. Des.*, Vol. 71, 342-344.

Luo, J.Y.; Gosman, A.D. & Issa, R.I. (1994). Prediction of impeller-induced flows in mixing vessels using multiple frames of reference. *Inst. Chem. Eng. Sympo. Ser.*, Vol. 136, 549-556.

Macosko, C.W. (1994). *Rheology: Principles, Measurements and Applications*, Wiley-VCH, New York.

Mavros, P.; Xuereb, C. & Bertrand, J. (1996). Determination of 3-D flow fields in agitated vessels by laser-doppler velocimetry. effect of impeller type and liquid viscosity on liquid flow patterns. *Chem. Eng. Res. Des.*, Vol. 74, 658-668.

McClements, D.J.; Povery, M.J.W. & Jury, M. (1990). Ultrasonic characterization of a food emulsion, *Ultrasonics*, Vol. 28, No. 4, 266-271.

Metzner, A.B. & Otto, R. E. (1957) Agitation of non-Newtonian fluids. *AIChE J.*, Vol. 3, No. 1, 3-10.

Mishra, V.P.; Dyster, K.N.; Jaworski, Z.; Nienow, A.W. & Mckemmie, J. (1998). A Study of an Up- and a Down-Pumping Wide Bade Hydrofoil Impeller: Part I. LAD Measurements, Can. J. Chem. Eng., Vol. 76, No. 3, 577-588.

Montante, G.; Mostek, M.; Jahoda, M. & Magelli. F. (2005). CFD Simulations and Experimental Validation of Homogenization Curves and Mixing Time in Stirred Newtonian and Pseudoplastic Liquids, Chem. Eng. Sci., Vol. 60, No. (8), 2427-2437.

Pakzad, L. (2007). Using Electrical Resistance Tomography (ERT) and Computational Fluid Dynamics (CFD) to Study the Mixing of Pseudoplastic Fluids with a Scaba 6SRGT Impeller. M.A.Sc. Thesis, Ryerson University, Toronto.

Pakzad, L.; Ein-Mozaffari, F. & Chan, P. (2008a). Using Electrical Resistance Tomography and Computational Fluid Dynamics Modeling to Study the Formation of Cavern in the Mixing of Pseudoplastic Fluids Possessing Yield Stress. Chem. Eng. Sci., Vol. 63, No. 9, 2508-2522.

Pakzad, L.; Ein-Mozaffari, F. & Chan, P. (2008b). Using Computational Fluid Dynamics Modeling to Study the Mixing of Pseudoplastic Fluids with a Scaba 6SRGT Impeller. Chem. Eng. Proc., Vol. 47, No. 12, 2218-2227.

Patel, H.; Ein-Mozaffari, F. & Upreti, S.R. (2008). Continuous Time Domain Characterization of Mixing in Agitated Pulp Chests. TAPPI J., Vol. 7, No. 5, 4-10.

Patwardhan, A.W. & Joshi, J.B. (1999). Relation between Flow Pattern and Blending in Stirred Tanks, Ind. Eng. Chem. Res., Vol. 38, No. 8, 3131-3143.

Paul, E.L.; Atiemo-Obeng, V. & Kresta, S.M. (2004). Handbook of industrial mixing: science & practice, Wiley-Interscience, New York.

Ranade, V.V. (1995). Computational Fluid Dynamics for Reactor Engineering. Rev. in Chem. Eng., Vol. 11, 229-284.

Ranade, V.V. (2002). Computational Flow Modeling for Chemical Reactor Engineering, Academic Press, San Diego.

Ranade, V.V. & Dommeti, S.M.S. (1996). Computational Snapshot of Flow Generated by Axial Impellers in Baffled Stirred Vessels. Chem. Eng. Res. Des., Vol. 74,476-484.

Renaud, M.; Belgacem, M.N.; Rinaudo, M. (2005). Rheological Behavior of Polysaccharide Aqueous Solutions. Polymer, Vol. 46, No. 4, 12348–12358.

Rutherford, K.; Mahmoudi, S.M.S.; Lee, K.C. & Yianneskis, M. (1996). The Influence of Rushton Impeller Blade and Disk Thickness on the Mixing Characteristics of Stirred Vessels. Chem. Eng. Res. Des., Vol. 74, 369-378.

Saeed, S. (2007). Dynamic and CFD Modeling of a Continuous-Flow Mixer Using Fluids with Yield Stress, M.A.Sc. Thesis, Ryerson University, Toronto.

Saeed, S.; Ein-Mozaffari, F. & Upreti, S.R. (2007). Using Computational Fluid Dynamics Modeling and Ultrasonic Doppler Velocimetry to Study Pulp Suspension Mixing. Ind. Eng. Chem. Res., Vol. 46, No. 7, 2172-2179.

Saeed, S. & Ein-Mozaffari, F. (2008). Using Dynamic Tests to Study the Continuous Mixing of Xanthan Gum Solutions. J. Chem. Technol. Biotechnol., Vol. 83, No. 4, 559-568.

Saeed, S.; Ein-Mozaffari, F. & Upreti, S.R. (2008). Using Computational Fluid Dynemics to Study the Dynamic Behavior of the Continuous Mixing of Herschel-Bulkley Fluids. Ind. Eng. Chem. Res., Vol. 47, No. 19, 7465-7475.

Sahu, A.K.; Kummar, P. & Joshi, J.B. (1998). Simulation of Flow in Stirred Vessels with Axial Flow Impellers: Zonal Modeling and Optimization of Parameter. Ind. Eng. Chem. Res., Vol. 37, No. 6, 2116-2130.

Solomon, J.; Elson, T.P. & Niewnow, A.W. (1981). Cavern Sizes in Agitated Fluids with a Yield Stress, Chem. Eng. Commun., Vol. 11, No. 1, 143-164.

Sommerfeld, M. & Decker, S., (2004). State of the Art and Future Trends in CFD Simulation of Stirred Vessel Hydrodynamics. Chem. Eng, Technol., Vol. 27, No. 3, 215-224.

Takeda, Y. (1986). Velocity Profile Measurement by Ultrasound Doppler Shift Method. Int. J. Heat Fluid Flow, Vol. 7, No. 4, 313-318.

Takeda, Y. (1991). Development of an Ultrasound Velocity Profile Monitor. Nucl. Eng. Des., Vol. 126, No. 2, 277-284.

Takeda, Y. (1995). Velocity Profile Measurement by Ultrasonic Doppler Method. Exp. Therm. Fluid Sci., Vol. 10, No. 4, 444-453.

Tatterson, G.B. (1991). Fluid Mixing and Gas Dispersion in Agitated Tanks, McGraw-Hill, Toronto.

Upreti, S.R. & Ein-Mozaffari, F. (2006). Identification of Dynamic Characterization Parameters of Agitated Pulp Chests Using a Hybrid Genetic Algorithm. Chem. Eng. Res. Des., Vol. 84, No. 3, 221-230.

Versteeg, H.K., & Malalasekera, W. (2007). An Introduction to Computational Fluid Mechanics – The Finite Volume Method, Pearson Prentice Hall, New York.

Whitcomb, P.J. & Macosko, C.W. (1978). Rheology of xanthan gum. J. Rheol., Vol. 22, No. 5, 493–505.

Wilkens, R.J.; Miller, J.D.; Plummer, J.R.; Dietz, D.C. & Myers, K.J. (2005). New Techniques for Measuring and Modeling Cavern Dimensions in a Bingham Plastic Fluid. Chem. Eng. Sci., Vol. 60, No. 19, 5269-5275.

Williams, R.P. (1986). On the Relationship between Velocity Distribution and Power Spectrum of Scattered Radiation in Doppler Ultrasound Measurements on Moving Suspensions, Ultrasonics, Vol. 24, No. 4, 197-200.

Wichterle, K. & Wein, O. (1975). Agitation of Concentrated Suspensions, Proceedings of CHISA 75, Paper B4.6, Prague, Czechoslovakia, 1975.

Xuewu, Z.; Xin, L.; Dexiang, G.; Wei, Z.; Tong, Z. & Yonghong, M. (1996). Rheological Models for Xanthan Gum. J. Food Eng., Vol. 21, No. 2, 203-209.

Yackel, D.C. (1990). Pulp and Paper Agitation: The History, Mechanics and Process, TAPPI Press, Atlanta.

Zlokarnik, M. (2001). Stirring: Theory and Practice, Wiley-VCH, Weinheim.
Zlokarnik, M. (2006). Scale-up in Chemical Engineering, Wiley-VCH, Weinheim.